Nuclear Engineering and Technology 50 (2018) 923–928

Contents lists available at ScienceDirect

Nuclear Engineering and Technology

journal homepage: www.elsevier.com/locate/net

Original Article

Investigation of nuclear material using a compact modified uniformly redundant array gamma camera

Taewoong Lee [a, b], Sung-Woo Kwak [c], Wonho Lee [d, *]

[a] Health Science Research Center, Korea University, 145, Anam-ro, Seongbuk-gu, Seoul, 02841, Republic of Korea
[b] RI Applied Research Team, Korea Institute of Radiologic and Medical Sciences, 75, Nowon-ro, Nowon-gu, Seoul, 01812, Republic of Korea
[c] Korea Institute of Nuclear Non-proliferation and Control, 1534, Yuseong-daero, Yuseong-gu, Daejeon 34054, Republic of Korea
[d] School of Health and Environmental Science, 145, Anam-ro, Seongbuk-gu, Seoul, 02841, Republic of Korea

ARTICLE INFO

Article history:
Received 1 September 2017
Received in revised form
28 March 2018
Accepted 4 April 2018
Available online 11 April 2018

Keywords:
Antimask Subtractive Method
Minimum Required Detection Time
Modified Uniformly Redundant Array Coded Aperture
UO_2 Pellet

ABSTRACT

We developed a compact gamma camera based on a modified uniformly redundant array coded aperture to investigate the position of a UO_2 pellet emitting characteristic X-rays (98.4 keV) and γ-rays (185.7 keV). Experiments using an only-mask method and an antimask subtractive method were conducted, and the maximum-likelihood expectation maximization algorithm was used for image reconstruction. The images obtained via the antimask subtractive method were compared with those obtained using the only-mask method with regard to the signal-to-noise ratio. The reconstructed images of the antimask subtractive method were superior. The reconstructed images of the characteristic X-rays and the γ-rays were combined with the obtained image using the optical camera. The combined images showed the precise position of the UO_2 pellet. According to the self-absorption ratios of the nuclear material and the minimum number of effective events for image reconstruction, we estimated the minimum detection time depending on the amount of nuclear material.

1. Introduction

Many kinds of γ-ray imaging systems combined with a visible-light camera have been used in homeland security and radioactive waste management applications for monitoring nuclear materials [1,2]. The most common imaging technique uses a pinhole or multihole collimator composed of a material with a high atomic number and high density [3,4]. These imaging systems provide excellent images at low energies (say, <200 keV) because the radiation attenuation caused by the collimator is inversely related to the radiation energy. However, as the radiation energy increases, the images become blurred and noisy owing to the penetration of the radiation through the collimator. Therefore, a thicker collimator is required, but this reduces the detection efficiency of the imaging system. To overcome this shortcoming, we must construct a collimator with a high efficiency, good image resolution, and minimal noise at various radiation energies.

Since Mertz and Young proposed the concept of a coded aperture to acquire radiation images in 1961 [5], many researchers have developed equipment that includes various types of coded apertures to maintain a high angular resolution and high signal-to-noise ratio (SNR). Several coded-aperture patterns are currently available, including the uniformly redundant array (URA) [6], the hexagonal URA [7], and the modified URA (MURA) [8]. The performance of the coded-aperture imaging system is better than that of the conventional pinhole collimator imaging system in environments with high background noise [6–9]. The URA exhibited a high SNR, but the horizontal and vertical lengths of URA are not equal; thus, it must be tightly coupled with a square-shaped photo device [6]. In addition, the structure of the URA mask is not antisymmetric on any mask rotation to use the antimask subtractive method. Hexagonal URA and MURA are antisymmetric on 60° and 90° rotation, respectively [7,8]. Hence, the antimask subtractive method can be applied for X-ray and γ-ray imaging to increase the SNR of the reconstructed image [10,11]. The sensitivity and SNR of the MURA are equal to that of the URA [8]. In addition, the square-shaped MURA array, which is commensurate with common photo devices, was demonstrated to be particularly popular [12]. Hence, the MURA was adopted for mechanical collimation in our detection system.

* *Corresponding author.*
E-mail address: wonhol@korea.ac.kr (W. Lee).

https://doi.org/10.1016/j.net.2018.04.006

Table 1
List of characteristic X-rays and γ-rays emitted from ^{235}U.

Radiation	Energy (keV)	Relative intensity (%)
K_α characteristic X-rays	94.7	50–53
	98.4	100
	111.3	~20
γ-rays	143.7	10.96
	185.7	57.2
	205.3	5.01

The purpose of this study was to develop a compact gamma camera with a MURA coded-aperture detection system and evaluate its performance in monitoring nuclear material such as a UO_2 pellet. To reduce the background noise by applying the antimask subtractive method, the reconstructed images were obtained using a mask that was antisymmetric for 90° rotation. The maximum-likelihood expectation maximization (MLEM) algorithm was used to obtain a sharper and more precise reconstructed image [13]. Finally, we estimated the minimum required detection time and count rate for various masses of nuclear material.

2. Material and methods

The major energy peaks of the K_α characteristic X-rays and γ-rays emitted from the ^{235}U are shown in Table 1. The highest yield of the characteristic X-rays and the γ-ray were at 98.4 and 185.7 keV, respectively [14,15]. Hence, radiation interaction events around the 98.4 and 185.7 keV peaks in the measured energy spectra were selected as effective data for the detection of the UO_2 pellet.

Fig. 1 shows the nuclear survey imaging system consisting of a MURA collimator, a CsI (Na) scintillator coupled to a position-sensitive photomultiplier tube (H8500), a front-end circuit, a field-programmable gate array (FPGA, SPARTAN 3E), and a data acquisition (DAQ) board (NI 9178). To determine the location of the γ-ray interaction in the CsI (Na) scintillator, four positioning signals were measured in the front-end circuit using a resistive charge divider. The FPGA and the DAQ board collected the timing and amplitude information, respectively. The FPGA triggered the DAQ board to select the effective photoelectric events and send them to a computer.

The plane of the UO_2 pellet was placed 50 cm from the detector. The CsI (Na) in the detector module was 20 × 20 voxels, where each voxel was 2 × 2 × 5 mm^3. The energy resolution of the pixelated CsI (Na) detector was approximately 12% at 662 keV. The open area of the MURA coded aperture through which radiation passed for γ-ray imaging was approximately 50% [8]. The MURA mask was made of tungsten and had dimensions of 73 × 73 × 5 mm^3, where each pixel was 2 × 2 × 5 mm^3. The mask-to-detector distance was 3 cm.

To reduce the background noise, we performed the experiments using the antimask. In the antimask subtractive method, all holes in the original only-mask pattern are replaced by opaque elements, as shown in Fig. 2, thus reducing the background noise of the subtracted shadow image [(only-mask) − (antimask)]. This leads to a higher quality reconstructed source image. To quantitatively evaluate the quality of the reconstructed images, the SNR was calculated as follows [8,9]:

$$\mathrm{SNR} = \frac{\bar{s}}{\sqrt{\sum (x_i - \bar{x})^2 / n}}, \tag{1}$$

where $\bar{s}$ represents the average value of the source pixels, including the maximum pixel; x_i and $\bar{x}$ represent the values of the pixels, excluding the source pixels, and the average of x_i, respectively; and n represents the number of pixels x_i. As explained previously, the effect of the antimask subtractive method on the quality of the reconstructed image was evaluated and is compared with that of the only-mask method in Section 3.

In the correlation reconstruction algorithm [8,9], the background noise is enhanced by the difference between the binary coded-aperture matrix and the real condition with a statistical fluctuation. However, the MLEM algorithm assuming a Poisson distribution can accurately model the experimental conditions. To determine the precise position and distribution of the radiation source, the MLEM algorithm was used for image reconstruction. The expectation maximization algorithm for radiation measurement application was derived by Lange and Carson [13]. The source distribution is estimated as follows [16]:

$$\lambda_j^{n+1} = \frac{\lambda_j^n}{\sum_i t_{ij}} \sum_i \frac{t_{ij} Y_i}{\sum_k t_{ik} \lambda_k^n}, \tag{2}$$

where n is the iteration number; λ_j^{n+1} and λ_j^n are the estimated values of a source pixel j after the $(n+1)^{th}$ and n^{th} iterations,

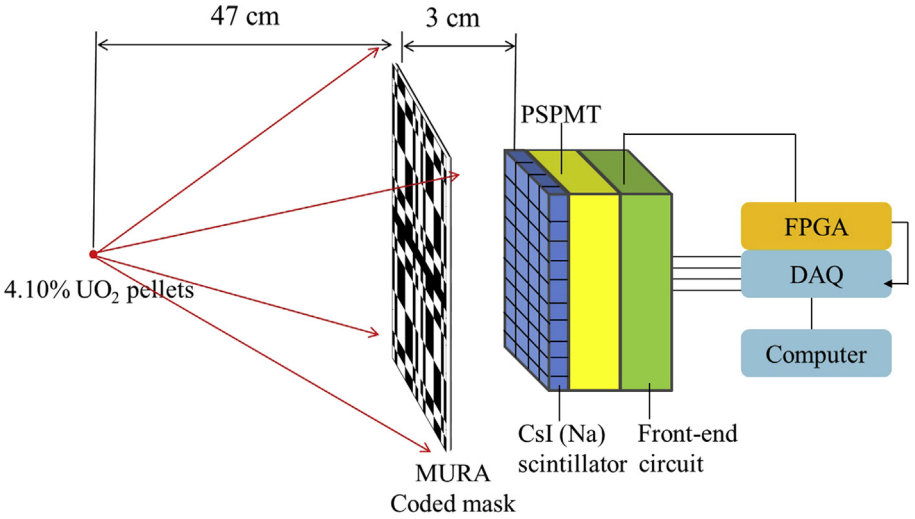

Fig. 1. Schematic representation of the nuclear survey imaging system.
DAQ, data acquisition; FPGA, field-programmable gate array; MURA, modified uniformly redundant array; PSPMT, position-sensitive photomultiplier tube.

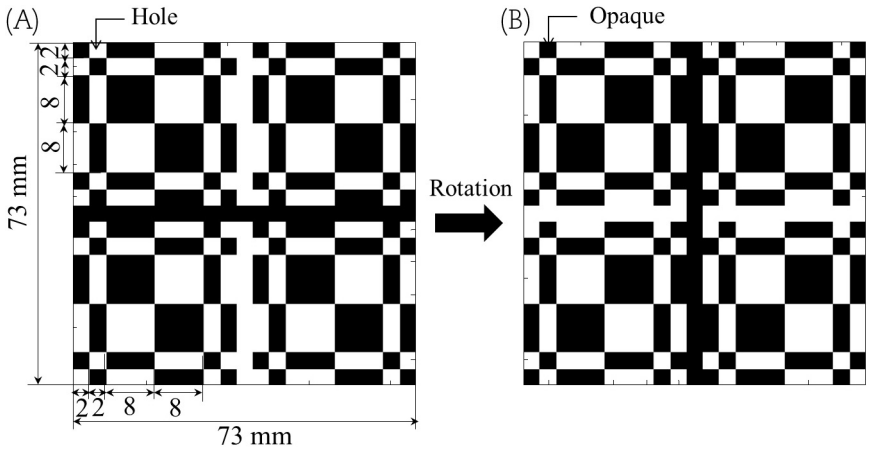

Fig. 2. Geometry of the MURA coded aperture used in the experiment. (A) Only-mask. (B) Antimask.
MURA, modified uniformly redundant array.

Table 2
Specifications of the optical camera.

Sensor vendor	Sony
Sensor	IMX240 BSI
Sensor type	CMOS
Sensor size	1/2.6 in
Pixels	16 megapixels

respectively; and t_{ij} is an element in the system matrix for the MURA coded aperture that consists of tungsten and air. In the only-mask method, Y_i is the shadow image of the MURA mask. In the antimask subtractive method, Y_i is the shadow image including the subtraction of background events, providing a high-quality reconstructed source image. As the iterations increased, the resolution of the reconstructed image improved, but the noise increased; hence, the 10^{th} iteration was chosen, in which the reconstructed image showed a high resolution without a significant noise peak.

Table 2 presents the specifications of the optical camera. The pixel size of each optical and coded-aperture image was approximately 0.0625 and 3.3 cm, respectively, for nuclear material at a distance of 50 cm. The source was located at the center of the two images. To construct the combined images, we adjusted the scale of the optical and γ-ray images according to the pixel size of each image and overlaid the images using MATLAB.

Fig. 3A shows the setup of the compact gamma camera with the MURA coded aperture used for the experiment. The UO_2 pellet had a diameter of 1 cm and a height of 1.5 cm, as shown in Fig. 3B. The total mass of the UO_2 pellet was 14.5 g, and the ^{235}U was enriched to 4.1%. The calculated activity of the ^{235}U was 1.14 μCi.

The radiation from the UO_2 pellet can be shielded by the pellet material. Several-millimeter UO_2 pellet can significantly absorb radiation from the center of the pellet, whereas the radiation emitted from the surface of the pellet can reach the gamma camera. Therefore, the self-absorption of γ-rays by their nuclear material source must be considered. Assuming that the nuclear material was spherical, the ratios of emitted radiation from the mass can be calculated using the following equations [17]:

$$R = \left(\frac{mass \times 3}{\rho \times 4\pi}\right)^{1/3} \tag{3}$$

$$\text{Emitted ratio} = \frac{\int_0^R S_0 e^{-\mu(R-r)} \times 4\pi r^2 dr}{\int_0^R 4\pi r^2 dr} = \frac{e^{-R}\left[\frac{2}{\mu^3} + \frac{e^{-\mu R}}{\mu} \times \left(R^2 + \frac{2R}{\mu} + \frac{2}{\mu^2}\right)\right]}{\frac{R^3}{3}}, \tag{4}$$

where ρ and μ represent the density and attenuation coefficient of ^{235}U at 185 keV, respectively, and S_0 represents the activity per unit volume. It was also assumed that the absolute counting efficiency was inversely proportional to the square of the distance between the source and gamma camera and that the source activity was proportional to the mass of the source.

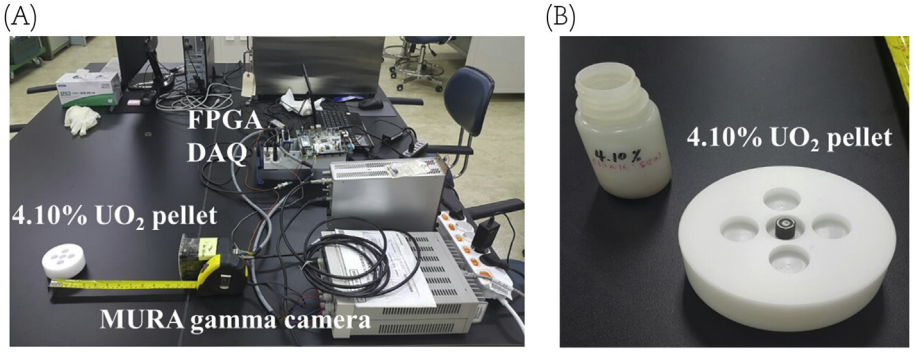

Fig. 3. (A) Nuclear survey imaging system. (B) UO_2 pellet.
DAQ, data acquisition; FPGA, field-programmable gate array; MURA, modified uniformly redundant array.

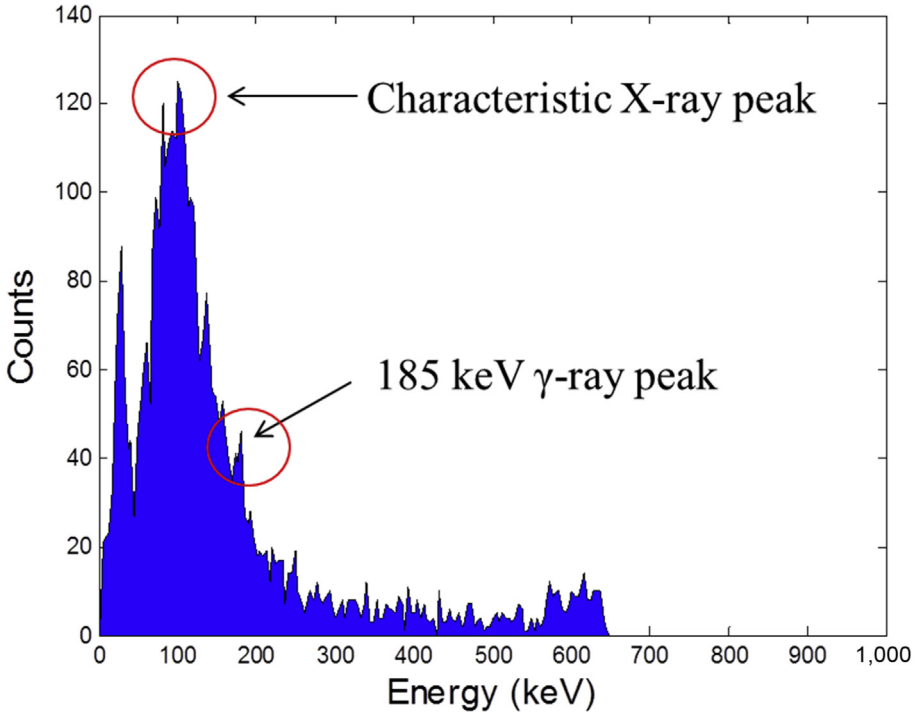

Fig. 4. Energy spectrum of the UO_2 pellet.

On the basis of the calculated self-absorption ratio and the minimum time needed to acquire effective events for image reconstruction, we estimated the minimum measurement time and count rate for various masses of ^{235}U. The results are discussed in Section 3.

3. Results

The energy spectrum measured by a single pixel of the CsI(Na) detector array is shown in Fig. 4. The characteristic X-ray peak at 98.4 keV and the γ-ray peak at 185.7 keV of ^{235}U were measured simultaneously. According to the peak information in each pixel of the detector, the characteristic X-ray and γ-ray energies were easily distinguished for image reconstruction.

The reconstructed images obtained using the MLEM algorithm for the characteristic X-rays (98.4 keV) and the 185.7 keV γ-rays emitted by ^{235}U are shown in Figs. 5 and 6, respectively. To obtain the reconstructed images using effective photoelectric events, energy windows of ±16% at 98.4 keV and ±11% at 185.7 keV were applied to each photoelectric peak. The size of reconstructed image pixel was 3.3 × 3.3 cm^2. The intrinsic imaging efficiency—i.e., the ratio of the number of effective events used for image reconstruction to the total number of γ-rays incident on the surface of the detector [18]—for the compact MURA gamma camera was 15.7 % at 185.7 keV.

The reconstructed images of Figs. 5A and 6A were obtained from measurements made without the antimask for 1 hour, those of Figs. 5B and 6B were obtained from measurements made without the antimask for 2 hour, and those of Figs. 5C and 6C were obtained from measurements made with the only-mask and antimask for 1 hour. All images reconstructed using the antimask subtractive method had less background noise than those reconstructed using only-mask measurements. Hence, the quality of the reconstructed images obtained using the antimask subtractive method was higher than that of the reconstructed images obtained using the only-mask method (Table 3). At lower radiation energies, the photoelectric effect is dominant, and the detector absorbs most of the radiation. Thus, our gamma camera was better

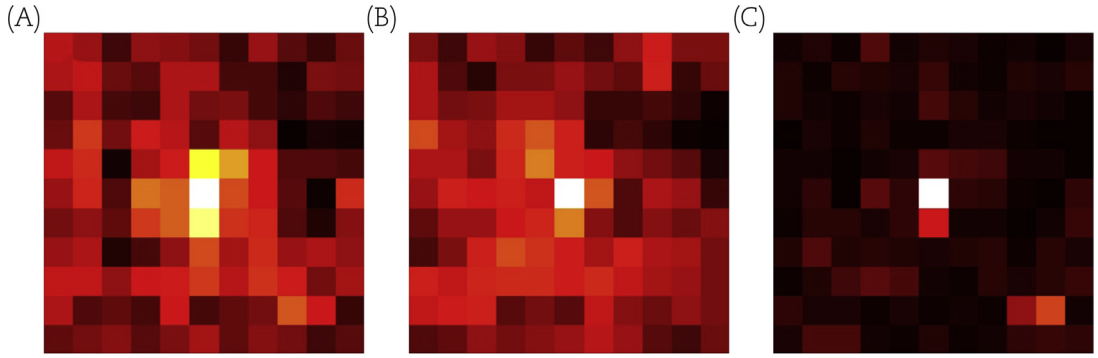

Fig. 5. Reconstructed images obtained using the MLEM algorithm (10 iterations) for 98.4-keV characteristic X-rays. (A) Only-mask method (measurement time = 1 h). (B) Only-mask method (measurement time = 2 h). (C) Antimask subtraction method (measurement time = 2 h).
MLEM, maximum-likelihood expectation maximization.

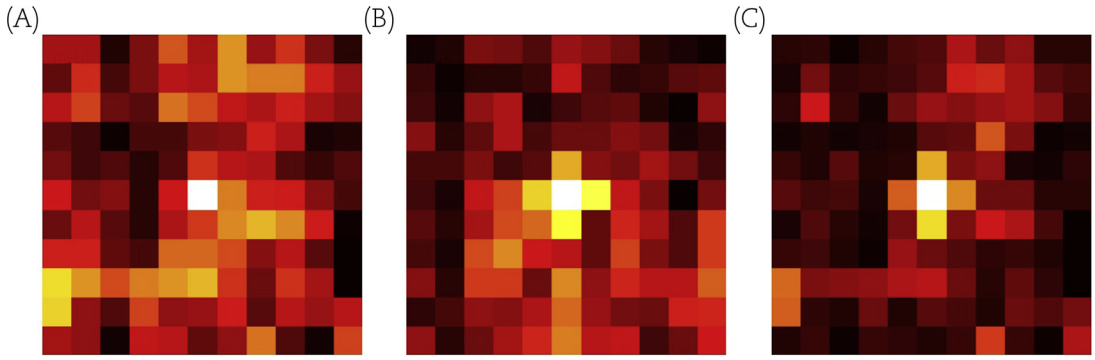

Fig. 6. Reconstructed images obtained using the MLEM algorithm (10 iterations) for 185.7-keV γ-rays. (A) Only-mask method (measurement time = 1 h). (B) Only-mask method (measurement time = 2 h). (C) Antimask subtraction method (measurement time = 2 h).
MLEM, maximum-likelihood expectation maximization.

Table 3
Performance comparison between the only-mask imager and the antimask imager.

Energy (keV)	Measurement method (measurement time)	SNR
Characteristic X-ray (98.4 keV)	Only-mask (1 h)	13.03
	Only-mask (2 h)	15.18
	Mask and Anti-mask (2 h)	16.13
γ-ray (185.7 keV)	Only-mask (1 h)	7.81
	Only-mask (2 h)	8.64
	Mask and Anti-mask (2 h)	8.82

SNR, signal-to-noise ratio.

at detecting the characteristic X-rays (98.4 keV) than the γ-rays (185.7 keV).

To verify the accuracy of the location of the UO_2 pellet and its radiation distribution, the reconstructed images of the characteristic X-rays and the γ-rays were combined with the image from the optical camera, as shown in Fig. 7. The combined images show the precise location of the UO_2 pellet and the radiation distribution.

A critical mass is the smallest amount of fissile material needed for a sustained nuclear chain reaction [19]. In general, the critical mass of spherical ^{235}U without a neutron reflector is approximately 50 kg. However, the critical mass of a nuclear material that includes neutron reflectors is smaller than that of the bare nuclear material [20]. The critical mass of spherical ^{235}U with a neutron reflector was approximately 15 kg. It is important to estimate the minimum measurement time and count rate according to this critical mass.

The time needed for the 4.10% UO_2 pellet to generate a reliable reconstructed image at the measurement distance of 50 cm was 1 hour. According to the measurement result and the calculation, including the relative distance between the source and gamma camera, the source activity, and the self-absorption in the spherical source, we estimated the minimum times and count rates. The conditions required to detect the various masses of 100 % ^{235}U, assumed to be 10 m from the detector, are shown in Figs. 8 and 9.

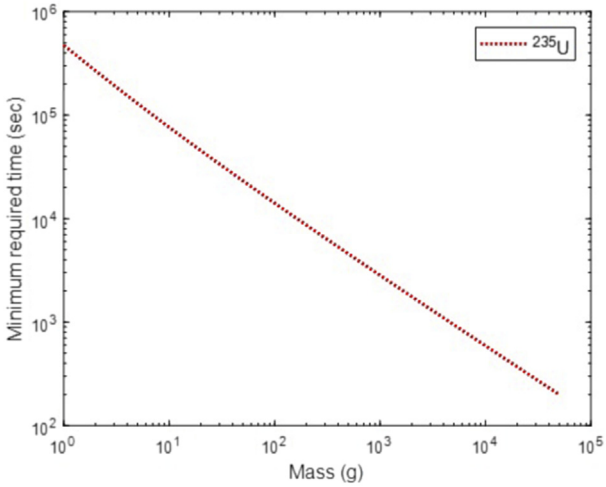

Fig. 8. Estimated minimum time needed for our system to detect ^{235}U at a 10-m distance.

Table 4 presents the minimum time and count rates required for our detection system to generate reconstructed images for the indicated critical mass of the nuclear material. As shown in the results, the estimated minimum times decreased with the increasing mass of the nuclear material.

4. Conclusions

We developed a gamma camera based on an only-mask and antimask mechanical system to investigate the location of a UO_2 pellet and its radiation distribution and then compared the reconstructed images obtained using these two methods with regard to the SNR. The MLEM method was used to reconstruct the only-mask and antimask images. The SNRs of the reconstructed

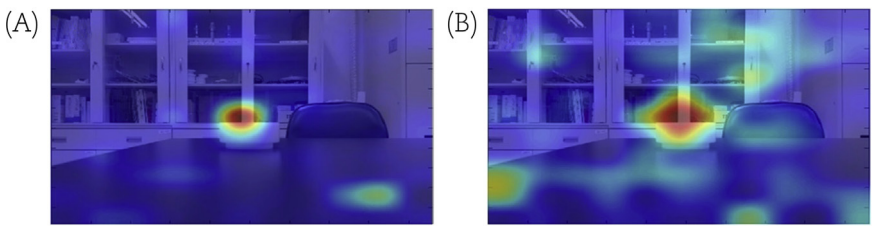

Fig. 7. Reconstructed images obtained using the antimask subtraction method and the MLEM algorithm method (10^{th} iteration) combined with the optical camera images. (A) Characteristic X-rays (98.4 keV). (B) γ-rays (185.7 keV).
MLEM, maximum-likelihood expectation maximization.

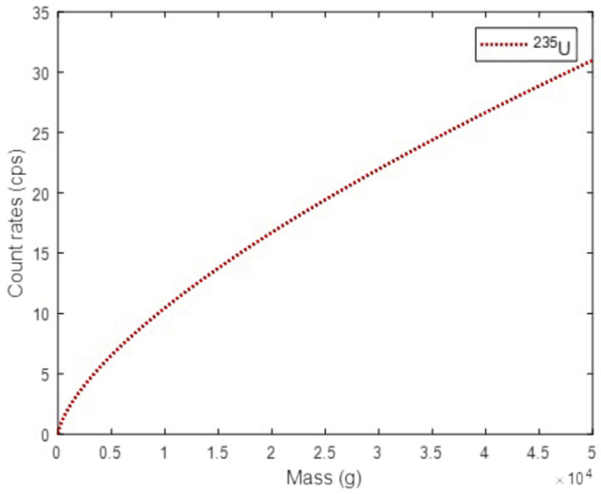

Fig. 9. Estimated count rate of ^{235}U at a 10-m distance.

Table 4
Estimation of the required detection time and count rate for the critical mass of ^{235}U at a 10-m distance from the camera.

Critical mass without neutron reflector (=50 kg)		Critical mass with neutron reflector (=15 kg)	
Required time (s)	Count rates (cps)	Required time (s)	Count rates (cps)
199.4 s	30.9 cps	448.9 s	13.8 cps

images were calculated for the characteristic X-rays and γ-rays from the UO_2 pellet. The images acquired using the antimask subtraction method were generally better than those acquired using the only-mask method. The estimated minimally required detection time and count rates showed the feasibility of using the MURA coded-aperture imaging system to monitor various radiation levels of ^{235}U.

Conflict of interest

There is no conflict of interest.

Acknowledgments

This work was supported by the Nuclear Safety Research Program through the Korea Foundation of Nuclear Safety (KoFONS) using financial resources granted by the Nuclear Safety and Security Commission (NSSC) of the Republic of Korea (No. 1603015) and by a grant from Korea University (K1711221).

References

[1] R. Redus, M. Squillante, J.S. Gordon, P. Bennett, G. Entine, An imaging nuclear survey system, IEEE Trans. Nucl. Sci. 43 (3) (1996) 1827–1831.
[2] M. Woodring, D. Beddingfield, D. Souza, G. Entine, M. Squillante, J. Christian, A. Kogan, Advanced multi-dimensional imaging of gamma-ray radiation, Nucl. Instrum. Methods Phys. Res. A 505 (2003) 415–419.
[3] W. Lee, G. Cho, Pinhole collimator design for nuclear survey system, Ann. Nucl. Energy 29 (2002) 2029–2040.
[4] S.V. Guru, Z. He, J.C. Ferreria, D.K. Wehe, G.F. Knoll, A high energy gamma camera using a multiple hole collimator and PSPMT, Nucl. Instrum. Methods Phys. Res. A 353 (1994) 328–333.
[5] L. Mertz, N.O. Young, Fresnel transformation of images, Proc. Intl. Conf. Opt. Instrum. (1961) 305–310.
[6] E.E. Fenimore, T.M. Cannon, Coded aperture imaging with uniformly redundant arrays, Appl. Opt. 17 (3) (1978) 337–347.
[7] W.R. Cook, M. Finger, T.A. Prince, E.C. Stone, Gamma-ray imaging with a rotating hexagonal uniformly redundant array, IEEE Trans. Nucl. Sci. NS-31 (1998) 771–775.
[8] S.R. Gottesman, E.E. Fenimore, New family of binary arrays for coded aperture imaging, Appl. Opt. 28 (20) (1989) 4344–4352.
[9] P.T. Durrant, M. Dallimore, I.D. Jupp, D. Ramsden, The application of pinhole and coded aperture imaging in the nuclear environment, Nucl. Instrum. Methods Phys. Res. A 422 (1999) 667–671.
[10] J. Braga, T. Villela, U.B. Jayanthi, F. D'Amico, J.A. Neri, A new mask-antimask coded-aperture telescope for hard X-ray astronomy, Exp. Astron. 2 (2) (1991) 101–113.
[11] R. Accorsi, F. Gasparini, R.C. Lanza, Optimal coded aperture patterns for improved SNR in nuclear medicine imaging, Nucl. Instrum. Methods Phys. Res. A 474 (2001) 273–284.
[12] M.J. Cieślak, K.A.A. Gamage, R. Glover, Coded-aperture imaging systems: past, present and future development – a review, Radiatt Meas. 92 (2016) 59–71.
[13] K. Lange, R. Carson, EM reconstruction algorithms for emission and transmission tomography, J. Comput. Assist. Tomogr 8 (2) (1997) 306–316.
[14] M.J. Berger, J.H. Hubbell, S.M. Seltzer, J. Chang, J.S. Coursey, R. Sukumar, D.S. Zucker, K. Olsen, XCOM: Photon Cross Sections Database, NBSIR 87–3597. Available at: www.nist.gov/pml/xcom-photon-cross-sections-database.
[15] W.D. Ruhter, R. Gunnink, Application of cadmium-zinc-telluride detectors in ^{235}U enrichment measurements, Nucl. Instrum. Methods Phys. Res. A 353 (1994) 716–718.
[16] T. Lee, W. Lee, Compact hybrid gamma camera with a coded aperture for investigation of nuclear materials, Nucl. Instrum. Methods Phys. Res. A 767 (2014) 5–13.
[17] J.P. Francois, On the calculation of the self-absorption in spherical radioactive sources, Nucl. Instrum. Methods Phys. Res. A 177 (1967) 153–156.
[18] G.F. Knoll, Radiation Detection and Measurement, fourth ed., Wiley, New York, 2010.
[19] R.Q. Richard, C.M. Hopper, Calculation of minimum critical mass of fissile nuclides, Nucl. Sci. Eng. 158 (2008) 203–209.
[20] M.S.E. Naschie, A. Hussein, On the eigenvalue of nuclear reaction and self-weight buckling, Chaos Solitons Fractals 11 (2000), 815–815.